Robotica (2002) volume 20, pp. 545–551. © 2002 Cambridge University Press
DOI: 10.1017/S0263574702004149 Printed in the United Kingdom

A mathematical model for a pneumatically actuated robotic fibre placement system

Gürsel Alici*, Bijan Shirinzadeh*, Andrew McConville*, Chee W. Foong* and Marcelo Ang†

(Received in Final Form: March 4, 2002)

SUMMARY

In this paper, a lumped parameter model of a robotic fibre placement system consisting of a Motoman SK-120 robot, a force/torque sensor, a pneumatic actuator and a stiff workpiece holder is developed and experimentally verified for the purpose of predicting and characterising the dynamic behaviour of the fibre placement system. Special attention has been given to the dynamics of the actuator which is represented as a mass confined to move between two non-linear springs and dampers. The overall model containing manipulator, force sensor, pneumatic actuator and the workpiece holder dynamics is of the tenth order. Step response experiments were conducted to verify the model and to determine the approximate values of the parameters in the mathematical model. The results prove that the established model is accurate enough to explain the dynamic behaviour of the fibre placement system and it can be employed to quantify the influence of the dynamics of the pneumatic actuator on the constant force-based fibre placement. The well-known fact that the dynamics of the pneumatic actuator varies with the piston position has also been experimentally demonstrated.

KEYWORDS: Pneumatic actuators; Mathematical modelling; Robotic fibre placement; Force sensing.

1. INTRODUCTION

Fibre reinforced composites offer the advantages of light-weight, high stiffness and high strength over traditional materials, such as steel and steel alloys, aluminium, brass, wood, etc., in many areas such as automotive, aerospace and sporting equipment. However, the traditional method of producing composites, usually known as manual fibre placement, is tedious, time consuming as well as labour intensive. Employing an industrial robot equipped with a specially designed fibre placement head can rectify these undesirable features. The robot is responsible for the accurate positioning and manipulation of the unit. The key element of the unit is a constant force pneumatic actuator that provides the compaction force needed. Although pneumatic actuation has been commonly used to generate motion between two hard stops, it is able to replace hydraulic and electric actuation in robotic contact task applications, where a source of compliance is needed to compensate for impulsive forces as well as to improve the stability of the system. The natural compliance of the compressed air can be exploited for contact applications. Justifications for this has been extensively discussed in the literature.[1–5]

When compared to hydraulic actuators, pneumatic actuators are simple, inexpensive, clean, easy to maintain, and have a high power to weight ratio.[6] On the other hand, the fundamental problems associated with pneumatic actuators are the compressibility of air, poor damping ability, significant mechanical friction, the time delay in system response due to stiction, pressure drop along transmission pipes, and other non negligible non-linearities, which change with time and operating conditions. Especially when using low-pressure air as the working medium, the non-linearities bring themselves forward in significant drift and hysteresis in the system, which affects the accuracy and repeatability. No matter what type of a pneumatic actuator (symmetric or asymmetric) is used, the response of a pneumatic system is dominated by the variation of leakage and friction in the cylinder with the piston position, compressibility of air, and a time constant, which indicates how fast air fills the cylinder.[7–10] Glass cylinders with graphite pistons have been employed to develop an air bearing between the piston and the cylinder, and hence friction and air leakage can be reduced significantly.[1]

In the literature, either state space models or linear transfer functions are used to mimic the behaviour of pneumatic systems about the mid-stroke operating point.[3,7,10–13] Due to the reasons presented above, pneumatic drives are inherently complex and difficult to model with any precision. However, it will be useful to develop just sufficiently accurate mathematical models in interpreting and characterising the behaviour of pneumatic servos rather than as an exact design tool.

In this paper, a lumped parameter model of the robotic fibre placement system based on a constant force pneumatic actuator is developed and the model parameters are obtained from comparing the simulated contact force to the actual force measured by a force/torque sensor. The results prove that the established model is accurate enough to represent the dynamic behaviour of the fibre placement head and it can be employed to quantify the influence of the dynamics of the pneumatic actuator on the force-based fibre

* Robotics & Mechatronics Research Laboratory, Department of Mechanical Engineering, Monash University, P.O. Box 31, Clayton, Victoria 3800 (Australia)
† National University of Singapore, Department of Mechanical and Production Engineering, 10 Kent Ridge Crescent, 119260 Singapore
E-mail: gursel.alici@eng.monash.edu.au

https://doi.org/10.1017/S0263574702004149 Published online by Cambridge University Press

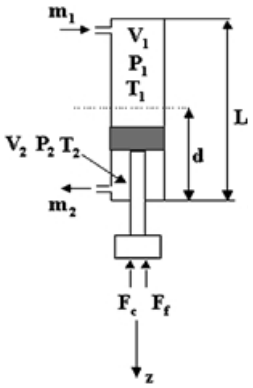


Fig. 1. Schematic of the pneumatic actuator.

placement. The well-known fact that the dynamics of the pneumatic actuator varies with the piston position has also been experimentally demonstrated.

2. MATHEMATICAL MODELLING OF A PNEUMATIC ACTUATOR

The manipulator translates the fibre placement head along the desired path in the plane of the workpiece holder and the pneumatic actuator supplies the compaction force needed. It must be re-emphasised that the response of such a system is dominated by the dynamics of the pneumatic actuator. Therefore, a special attention is given to the actuator dynamics. Many researchers have reported on the dynamics analysis of pneumatic actuators before.[1,3,4,6,7,10,11] A similar analysis is given below for the sake of completeness. Consider an asymmetric pneumatic actuator driven with a four-way valve, shown in Figure 1. It is assumed that the piston is moving downwards. An equivalent mass, non-linear spring and a damper system can represent this combination. Thus, the equation of motion for the system is:

$$\mathbf{m_e}\frac{\mathbf{d^2z}}{\mathbf{dt^2}}+\mathbf{b_e}\frac{\mathbf{dz}}{\mathbf{dt}}=\mathbf{A_1P_1}-\mathbf{A_2P_2}-\mathbf{F_c}-\mathbf{F_f} \qquad (1)$$

where $\mathbf{m_e}$ is the lumped mass of the piston, rod and the fiber placement head in the vertical direction, $\mathbf{b_e}$ is the viscous damping coefficient,* $\mathbf{A_1}$ and $\mathbf{A_2}$ are the areas of the piston, $\mathbf{P_1}$ and $\mathbf{P_2}$ are the pressures in the chambers 1 and 2, $\mathbf{F_c}$ is the contact force between the fiber placement head and the workpiece, and $\mathbf{F_f}$ is friction force or any disturbance force acting on the end point along the z axis.

The equations of state for ideal gas in the chambers 1 and 2 are

$$\mathbf{P_1}=\rho_1\mathbf{RT_1},\quad \mathbf{P_2}=\rho_2\mathbf{RT_2} \qquad (2)$$

where ρ_1 and ρ_2 are the air densities, $\mathbf{R}$ is the gas constant, and $\mathbf{T_1}$ and $\mathbf{T_2}$ are the air temperatures in the chambers. The volumes $\mathbf{V_1}$ and $\mathbf{V_2}$ of the chambers can be expressed as follows:

* Although air provides little damping, it is included in the model for completeness.

$$\mathbf{V_1}=\mathbf{A_1}\left(\frac{\mathbf{L}}{\mathbf{2}}+\mathbf{z}\right),\quad \mathbf{V_2}=\mathbf{A_2}\left(\frac{\mathbf{L}}{\mathbf{2}}-\mathbf{z}\right) \qquad (3)$$

where $\mathbf{L}$ is the stroke of the cylinder and $\mathbf{z}$ is the displacement of the piston from the mid stroke. The mass $\mathbf{m_1}$ and $\mathbf{m_2}$ of the air in the respective chambers are:

$$\mathbf{m_1}=\mathbf{V_1}\rho_1,\quad \mathbf{m_2}=\mathbf{V_2}\rho_2 \qquad (4)$$

By substituting Equation 2, Equation 3 and Equation 4 into Equation 1, the following equation is obtained:

$$\mathbf{m_e}\frac{\mathbf{d^2z}}{\mathbf{dt^2}}+\mathbf{b_e}\frac{\mathbf{dz}}{\mathbf{dt}}+\underbrace{\frac{\mathbf{R}}{\mathbf{d^2}}\left(\frac{\mathbf{m_1T_1}+\mathbf{m_2T_2}}{\mathbf{1}-\frac{\mathbf{z^2}}{\mathbf{d^2}}}\right)}_{\mathbf{k_e}}\mathbf{z}=\frac{\mathbf{R}}{\mathbf{d}}\left(\frac{\mathbf{m_1T_1}-\mathbf{m_2T_2}}{\mathbf{1}-\frac{\mathbf{z^2}}{\mathbf{d^2}}}\right)-\mathbf{F_c}-\mathbf{F_f} \qquad (5)$$

where $\mathbf{d}$ is the half of the stroke. It must be noted that the expression on the right-hand side of Equation 5 represents the net force driving the piston and that $\mathbf{k_e}$ denotes the equivalent spring constant of two springs corresponding to

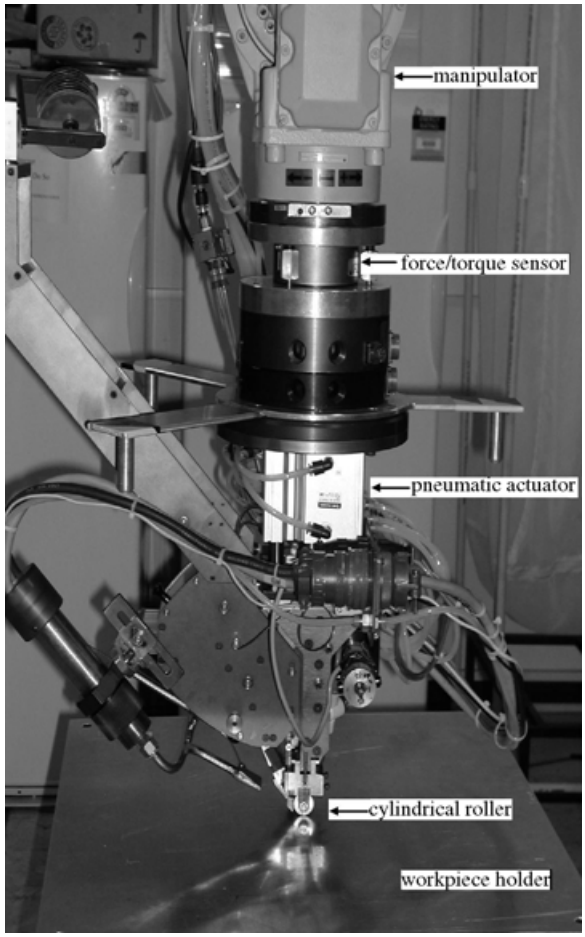


Fig. 2. Experimental step up for model verification.

https://doi.org/10.1017/S0263574702004149 Published online by Cambridge University Press

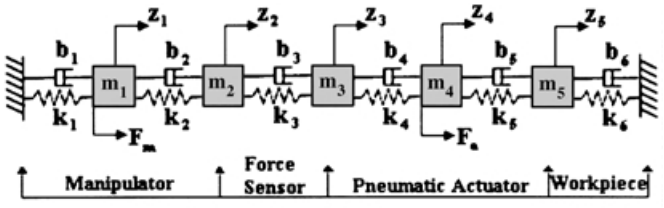


Fig. 3. Lumped parameter model of the fibre placement head in the **z** direction.

the air filled in the chambers **1** and **2**. This equivalent spring constant can be rewritten as:

$$\mathbf{k_e = k_1 + k_2 = \frac{m_1 R T_1}{d^2 - z^2} + \frac{m_2 R T_2}{d^2 - z^2}} \tag{6}$$

As given in Equation 6, the equivalent spring constant is a function of the mass, the temperature of the air and the position of the piston from the mid-stroke.[2,7,12] It is practically impossible to measure these quantities in order to evaluate the equivalent stiffness. However, it must be noted that when the piston approaches the mid of the stroke, the equivalent spring constant has a minimum value. On the other hand, while the piston is approaching the upper and lower dead positions, $\mathbf{k_e}$ tends to approach infinity.

If the pressures $\mathbf{P_1}$ and $\mathbf{P_2}$ in Equation 1 are known, the dynamic behaviour of the actuator can be analysed using Equation 1. The approximate pressure dynamics are given in references [1,4,6] and are depicted here for completeness:

$$\mathbf{P_1 = P_s(1 - e^{-(t/\tau_1)}) + P_1(0)e^{-(t/\tau_1)}} \tag{7}$$

$$\mathbf{P_2 = P_2(0)e^{-(t/\tau_2)}} \tag{8}$$

where $\mathbf{P_s}$ is the supply pressure and $\mathbf{P_1(0)}$ and $\mathbf{P_2(0)}$ are the initial pressures in the chambers 1 and 2 and they are almost equal to each other. The time constants τ_1 and τ_2 are expressed as:

$$\tau_1 = \frac{\mathbf{A_1 z}}{\mathbf{C_v R T_1}} \quad \text{and} \quad \tau_2 = \frac{\mathbf{A_2 (d - z)}}{\mathbf{C_v R T_2}} \tag{9}$$

where $\mathbf{C_v}$ is the coefficient of specific heat. So, the pressure difference driving the actuator is:

$$\underbrace{\mathbf{P_1 - P_2}}_{\Delta P} = \mathbf{P(0)(e^{-(t/\tau_1)} - e^{-(t/\tau_2)}) + P_s(1 - e^{-(t/\tau_1)})} \tag{10}$$

As the time t approaches infinity, the pressure difference is equivalent to the supply pressure. In many applications, the pressure difference is monitored by an analogue pressure regulator system that sends a control signal to the servo-valve to produce the desired pressure difference. It is well known that there are basically two time delays in a physical pneumatic system; the delay between the piston and the pressure transducer, and the delay between the valve and the piston. The latter determines how quickly the cylinder fills with air and therefore dominates the behaviour of a pneumatic actuator. In the light of this, the transfer function relating the pressure difference $\mathbf{\Delta P}$ driving the actuator to a desired pressure difference $\mathbf{\Delta P_d}$ is given as:[3,4,11,13]

$$\frac{\mathbf{\Delta P}}{\mathbf{\Delta P_d}} = \frac{\mathbf{1}}{\tau \mathbf{s} + \mathbf{1}} \tag{11}$$

where τ is a global time constant for the pressure control system, which is a pressure regulator for the fibre placement head considered in this study, and is an indication of how fast the regulator takes an action to build up a desired pressure in the cylinder. This follows that the actuator force $\mathbf{F_a(s)}$ in Equation 14 can be evaluated from:

$$\mathbf{F_a(s) = A_1 \times \Delta P_d \times \left(\frac{1}{\tau s + 1} \right)} \tag{12}$$

It was claimed that the time delay at room temperature and atmospheric pressure for the air with the density of **1.27 kg/m^3** is three milliseconds per meter of pipe length.[11] In another study,[14] it was found that the time delay was in the order of **0.01 sec**. As presented in Section 4, the time delay in our experimental system was as high as **0.09 second**.

3. MATHEMATICAL MODEL OF FIBER PLACEMENT HEAD

The fibre placement system consisting of a Motoman SK-120 robot, a wrist force/torque sensor sensor, an asymmetrical pneumatic actuator and a stiff workpiece holder is shown in Figure 2. Although the base on which the manipulator is installed is very stiff, the dynamics of the base is represented by a spring with a stiffness of $\mathbf{k_1}$ and a damper with a damping coefficient of $\mathbf{b_1}$ for the sake of completeness and generality. Since there might be many sources of flexibility in the structure of a typical manipulator, it is a common practice[15,16] to mimic the dynamic behaviour of a manipulator with two masses, $\mathbf{m_1}$ and $\mathbf{m_2}$, connected to each other through a damper and a spring. The spring constant $\mathbf{k_2}$ together with the damping coefficient $\mathbf{b_2}$ reflects the dynamics of the manipulator in the **z** direction. The stiffness constant can be due to the structural stiffness of the manipulator, position gains or the stiffness of transmission and drive train or the combination of these.

Similarly, the damping is a combination of the viscous joint damping and active damping from joint space into Cartesian space. A force sensor can exhibit its dynamics, especially when it is in contact with a stiff environment and/or impacts with a stiff environment. The same argument is also valid for an environment impacted by a very stiff robotic system. Therefore, the sensor and the workpiece dynamics are separately represented by a spring and a damper. As demonstrated experimentally in Section 4, the dynamics of the fibre placement head is dominated by the dynamics of the pneumatic actuator. The actuator dynamics are given by Equation 5, from which it is obvious that the actuator can be represented by a single mass connected to the force sensor and the workpiece holder with a spring and a damper. If the individual lumped parameter models of the

https://doi.org/10.1017/S0263574702004149 Published online by Cambridge University Press

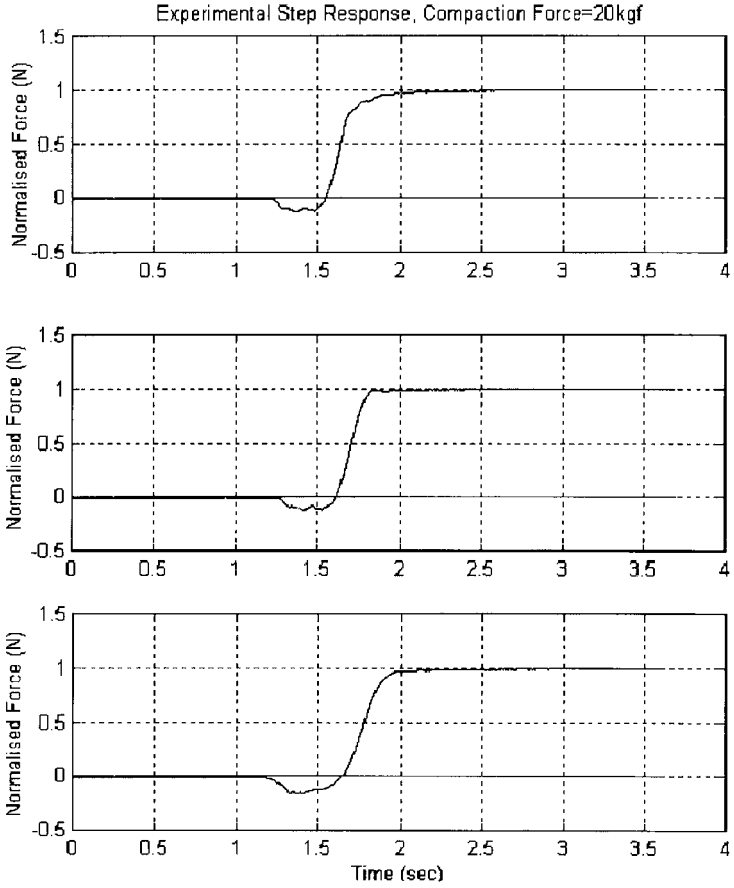


Fig. 4. Experimental step responses. The top, middle and bottom plots show the step responses for the upper-dead, mid-stroke and lower-dead positions of the piston, respectively.

manipulator, the force sensor, the actuator and the environment are combined; the model shown in Figure 3 is established. The force $\mathbf{F_m}$ denotes the force driving the manipulator in the **z**-axis direction. Since the manipulator is responsible for the motion in the **x-y** plane of the workpiece holder during a fibre placement operation, $\mathbf{F_m = 0}$. For the experimental results presented in the next section, a constant force was applied to the workpiece in the **z** direction only by the pneumatic actuator while the manipulator was kept at halt.

The open loop transfer functions for the model in Figure 3 are obtained as:

$$\frac{\mathbf{Z_1(s)}}{\mathbf{F_a}} = \frac{\mathbf{N_1(s)}}{\mathbf{D(s)}},$$

$$\frac{\mathbf{Z_2(s)}}{\mathbf{F_a}} = \frac{\mathbf{N_2(s)}}{\mathbf{D(s)}},$$

$$\frac{\mathbf{Z_3(s)}}{\mathbf{F_a}} = \frac{\mathbf{N_3(s)}}{\mathbf{D(s)}}, \qquad (13)$$

$$\frac{\mathbf{Z_4(s)}}{\mathbf{F_a}} = \frac{\mathbf{N_4(s)}}{\mathbf{D(s)}},$$

$$\frac{\mathbf{Z_5(s)}}{\mathbf{F_a}} = \frac{\mathbf{N_5(s)}}{\mathbf{D(s)}},$$

where

$$\begin{aligned}\mathbf{D(s)} = {} & [m_1s^2+(b_1+b_2)s+(k_1+k_2)][b_3s+k_3]^2[b_5s+k_5]^2 \\ & +[m_3s^2+(b_3+b_4)s+(k_3+k_4)][b_2s+k_2]^2[b_5s+k_5]^2 \\ & +[m_1s^2+(b_1+b_2)s+(k_1+k_2)][m_2s^2+(b_2+b_3)s+(k_2+k_3)] \\ & \times[m_3s^2+(b_3+b_4)s+(k_3+k_4)][b_5s+k_5]^2 \\ & +[m_5s^2+(b_5+b_6)s+(k_5+k_6)][b_2s+k_2]^2[b_4s+k_4]^2 \\ & +[m_1s^2+(b_1+b_2)s+(k_1+k_2)][m_2s^2+(b_2+b_3)s+(k_2+k_3)] \\ & \times[m_5s^2+(b_5+b_6)s+(k_5+k_6)][b_4s+k_4]^2 \\ & +[m_1s^2+(b_1+b_2)s+(k_1+k_2)][m_4s^2+(b_4+b_5)s+(k_4+k_5)] \\ & \times[m_5s^2+(b_5+b_6)s+(k_5+k_6)][b_3s+k_3]^2 \\ & +[m_3s^2+(b_3+b_4)s+(k_3+k_4)][m_4s^2+(b_4+b_5)s+(k_4+k_5)] \\ & \times[m_5s^2+(b_5+b_6)s+(k_5+k_6)][b_2s+k_2]^2 \\ & +[m_1s^2+(b_1+b_2)s+(k_1+k_2)][m_2s^2+(b_2+b_3)s+(k_2+k_3)] \\ & \times[m_3s^2+(b_3+b_4)s+(k_3+k_4)][m_4s^2+(b_4+b_5)s+(k_4+k_5)] \\ & \times[m_5s^2+(b_5+b_6)s+(k_5+k_6)]\end{aligned}$$

$$\begin{aligned}\mathbf{N_1(s)} = {} & -[m_5s^2+(b_5+b_6)s+(k_5+k_6)][b_2s+k_2][b_3s+k_3] \\ & [b_4s+k_4]\end{aligned}$$

$$\begin{aligned}\mathbf{N_2(s)} = {} & [m_1s^2+(b_1+b_2)s+(k_1+k_2)][m_5s^2+(b_5+b_6)s \\ & +(k_5+k_6)][b_3s+k_3][b_4s+k_4]\end{aligned}$$

$$\begin{aligned}\mathbf{N_3(s)} = {} & -[m_5s^2+(b_5+b_6)s+(k_5+k_6)][b_2s+k_2][b_4s+k_4] \\ & -[m_1s^2+(b_1+b_2)s+(k_1+k_2)]\times[m_2s^2+(b_2+b_3)s \\ & +(k_2+k_3)][m_5s^2+(b_5+b_6)s+(k_5+k_6)][b_4s+k_4]\end{aligned}$$

https://doi.org/10.1017/S0263574702004149 Published online by Cambridge University Press

Table I. Values of the parameters in the model for the three positions of the piston.

	m_i, (i=1, ··· 5) kg	b_i, (i=1, ··· 6) N s/m	k_i, (i=1, ··· 6) N/m
Upper-dead	30, 20, 12, 14, 10.5	1500, 1400, 1300, 210, 100, 350	300000, 200000, 400000, 21000, 10000, 150000
Mid-stroke	30, 20, 12, 14, 10.5	1500, 1400, 1300, 115, 100, 350	300000, 200000, 400000, 15000,11000,150000
Lower-dead	30, 20, 12, 14, 10.5	1500, 1400, 1300, 275, 300, 350	300000, 200000, 400000, 20000, 12000, 150000

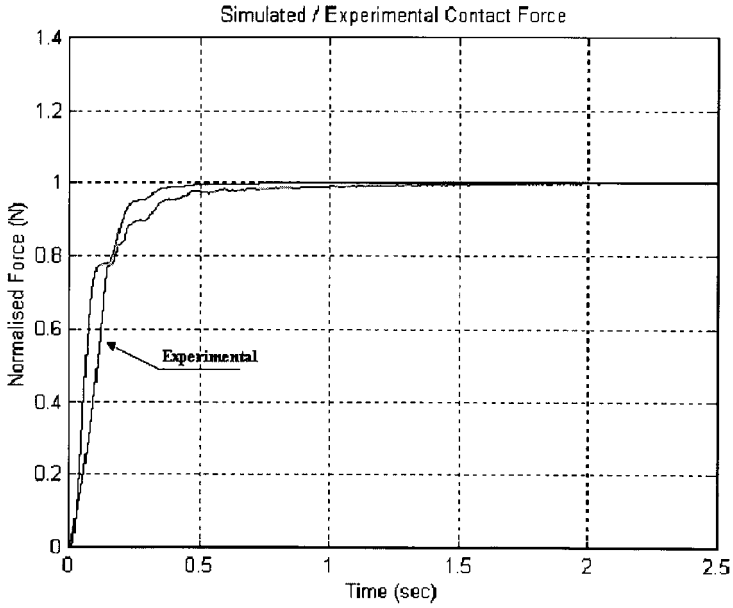


Fig. 5. Experimental and simulated step responses for the upper-dead position of the piston.

$$\begin{aligned}N_4(s)=&[m_1s^2+(b_1+b_2)s+(k_1+k_2)][m_5s^2+(b_5+b_6)s+(k_5+k_6)]\\&[b_3s+k_3]^2+[m_3s^2+(b_3+b_4)s+(k_3+k_4)]\\&[m_5s^2+(b_5+b_6)s+k_5+k_6)][b_2s+k_2]^2\\&+[m_1s^2+(b_1+b_2)s+(k_1+k_2)][m_2s^2+(b_2+b_3)s+k_2+k_3)]\\&\times[m_3s^2+(b_3+b_4)s+(k_3+k_4)][m_5s^2+(b_5+b_6)s\\&+(k_5+k_6)]\end{aligned}$$

$$\begin{aligned}N_5(s)=&[m_1s^2+(b_1+b_2)s+(k_1+k_2)][b_3s+k_3]^2[b_5s+k_5]\\&+[m_3s^2+(b_3+b_4)s+(k_3+k_4)][b_2s+k_2]^2[b_5s+k_5]\\&+[m_1s^2+(b_1+b_2)s+(k_1+k_2)][m_2s^2+(b_2+b_3)s\\&+(k_2+k_3)]\times[m_3s^2+(b_3+b_4)s+(k_3+k_4)][b_5s+k_5]\end{aligned}$$

The contact force measured by the force/torque sensor is $F_c(s)=k_3(Z_2(s)-Z_3(s))$ from which the open loop transfer function between the actuator force $F_a(s)$ and $F_c(s)$ is obtained as:

$$\frac{F_c(s)}{F_a(s)}=k_3\frac{N_2(s)-N_3(s)}{D} \tag{14}$$

4. VERIFICATION OF MATHEMATICAL MODEL

The experimental set up shown in Figure 2 includes a Motoman SK-120 robot, a JR3 force/torque sensor, a pneumatic actuator in contact with a very stiff worktable through a cylindrical steel roller. A pressure regulator controlled the desired force in the **z** direction, which was set at 20 kgf ($\approx$ 196 N). The pneumatic actuator embodies an SMC compact guide cylinder with a bore diameter of 32 mm, a piston area of **804 mm^2**, and a stroke of 100 mm.

Step response tests were accomplished to experimentally verify the mathematical model. The experimental (normalised) step responses of the manipulator in the vertical direction, shown in Figure 4, are for three different locations of the piston – upper dead, mid-stroke lower dead positions. The coefficients in the lumped parameter model expressed by Equation 13 are heuristically selected such that the simulated step response of the contact force calculated from Equation 14 fits these experimental step responses measured by the force sensor. The values of the parameters in the model are depicted in Table I for the three positions of the piston. It must be noted that the actuator dynamics represented by k_4, b_4, k_5, b_5, dominate the contact behaviour of the system.

As shown in Figures 5, 6 and 7, the normalised step response of the model matches the experimental step response quite well. It must be emphasised that the stiffness and damping coefficients for the pneumatic actuator depend on the position of the piston. When the piston is at the upper dead point, the response contains some oscillations, see

https://doi.org/10.1017/S0263574702004149 Published online by Cambridge University Press

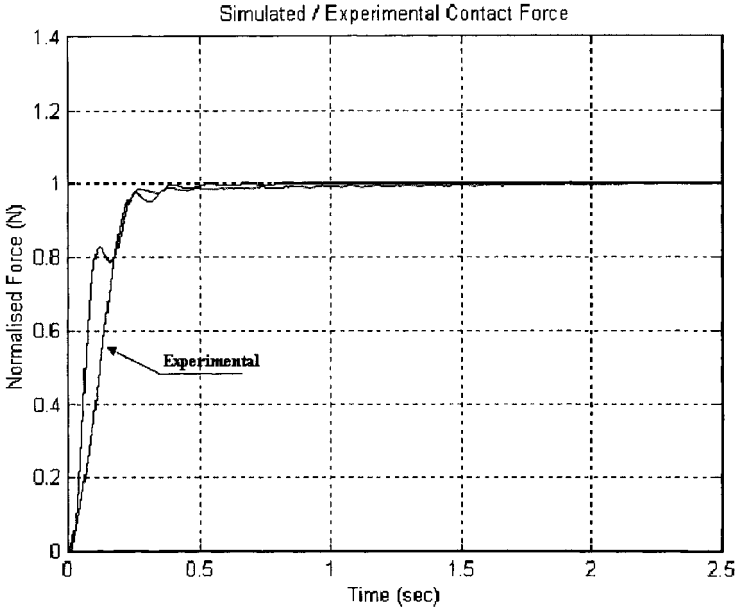


Fig. 6. Experimental and simulated step responses for the mid-stroke position of the piston.

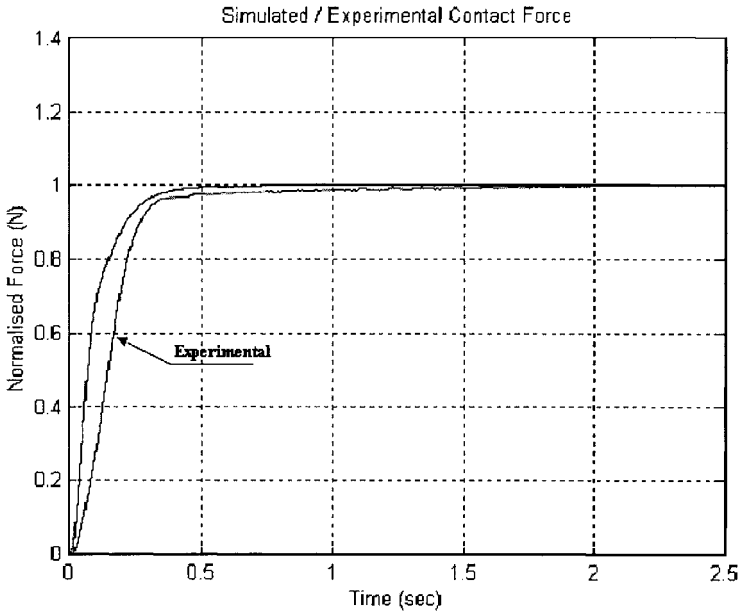


Fig. 7. Experimental and simulated step responses for the lower-dead position of the piston.

Figure 5. This could be due to the unpressurised air in the lower portion of the cylinder. Drawing the same analogy, when the piston is at the lower dead point, there exists no unpressurised air in the cylinder and therefore, the step response does not contain any oscillations, see Figure 7. On the other hand, when the piston is at the mid stroke, the response contains little oscillations when compared to the upper dead position, see Figure 6. As expected, the effective stiffness, $\mathbf{k_4}+\mathbf{k_5}$, at the mid stroke position is smaller than those at the upper and lower dead positions, see Table I. It was found that the time constant for all of the experimental results was of the order of 0.09 second, which is significantly large. Since the bore diameter and the stroke of the actuator were not large enough, the time constant did not change with the position of the piston. But, the stiffness and damping constants of the pneumatic system changed with the piston position.

5. CONCLUSIONS

In this study, a tenth-order lumped parameter model of the robotic fibre placement system has been developed. Step response experiments were conducted in order to verify the model and to evaluate the approximate numerical values for the parameters in the model. The experimental force step response is compared to the simulated response such that a close correspondence between them can be obtained. The results prove that the established model is accurate enough to represent the dynamic behaviour of the fibre placement system and it can be employed to quantify the influence of

https://doi.org/10.1017/S0263574702004149 Published online by Cambridge University Press

the dynamics of the pneumatic actuator on the constant force-based fibre placement. The well-known fact that the dynamics of the pneumatic actuator varies with the piston position has also been demonstrated experimentally.

Acknowledgement
This project has been partly funded by Australian Research Council (ARC).

References

1. A. K. Paul, J. K. Mishra and M. G. Radke, "Reduced order sliding mode control for pneumatic actuator", *IEEE Transactions on Control Systems Technology* **2**(3), 271–276 (September, 1994).
2. J. E. Bobrow and B. W. McDonell, "Modeling, identification, and control of a pneumatically actuated, force controllable robot", *IEEE Transactions on Robotics and Automation* **14**(5), 732–742 (October, 1998).
3. S. Liu and J. E. Bobrow, "An analysis of a pneumatic servo system and its application to a computer-controlled robot", *ASME Journal of Dynamic Systems, Measurement, and Control* **110**, 228–235 (September, 1988).
4. G. H. Pfreundschuh, V. Kumar and T. G. Sugar, "Design and control of a 3 DOF in-parallel actuated manipulator", *Proceedings of the 1991 IEEE International Conference on Robotics and Automation*, Sacramento, California (April, 1991) pp. 1659–1664.
5. R. B. Van Varseveld and G. M. Bone, "Accurate position control of a pneumatic actuator using on/off solenoid valves", *IEEE/ASME Transactions on Mechatronics* **2**(3), 195–204 (September, 1997).
6. B. W. Andersen, The Analysis and Design of Pneumatic Systems (John Wiley and Sons, 1967).
7. J. Pu and R. H. Weston, "A new generation of pneumatic servos for industrial robots", *Robotica* **7**, Part 1, 17–23 (1989).
8. J. A. Merchant, M. J. Street, P. Gurney and J. A. Benson, "Design and testing of a servo controller for pneumatic cylinders", *Proc. Inst. Mech. Eng. E* **203**, 21–27 (1989).
9. J. A. Linnett and M. C. Smith "An accurate low-friction pneumatic position control system", *Proc. Inst. Mech. Eng. B* **203**, 159–165 (1989).
10. S. Kawamura, K. Miyata, H. Hanafusa and K. Isida, "PI type hierarchical feedback control scheme for pneumatic robots", *Proceedings of the 1989 IEEE International Conference on Robotics and Automation* (1989) pp. 1853–1858.
11. J. J. Mannetje, "Pneumatic servo design method improves system bandwidth twenty-fold", *Control Engineering* 79–83 (June, 1981).
12. J. Pu, R. H. Weston and P. R. Moore, "Digital motion control and profile planning for pneumatic servos", *ASME Journal of Dynamic Systems, Measurement, and Control* **114**, 634–640 (December, 1992).
13. J. E. Bobrow and F. Jabbari, "Adaptive pneumatic force actuation and position control", *ASME Journal of Dynamic Systems, Measurement, and Control* **113**, 267–272 (June, 1991).
14. L. Guvenc and K. Srinivasan, "Modeling and parameter identification of a pneumatic constant force device", *Journal of Engineering and Environmental Sciences* **24**, 383–399 (2000).
15. G. Alici and R. W. Daniel, "Static Friction Effects during Hard-on-Hard Contact Tasks and Their Implications for Manipulator Design." *Int. J. Robotics Research* **13**(6), 508–520 (December, 1994).
16. G. Alici and R. W. Daniel, "Development and Verification of a Mathematical Model for Robot Force Control via Measuring an Input/Output Relationship and Force Control Experiments." *Int. J. Modelling and Simulation* **17**(2), 107–119 (1997).

https://doi.org/10.1017/S0263574702004149 Published online by Cambridge University Press